




Ultra-low dielectric constant and high thermal stability of low-crosslinked polyimide with zinc tetraamino phthalocyanine

Yang Zhang¹, Jiyu He^{1,*} , and Rongjie Yang¹

¹ National Engineering Research Center of Flame Retardant Materials, School of Materials Science & Engineering, Beijing Institute of Technology, Beijing 100081, People's Republic of China

Received: 22 May 2022

Accepted: 14 August 2022

Published online:

23 August 2022

© The Author(s), under exclusive licence to Springer Science+Business Media, LLC, part of Springer Nature 2022

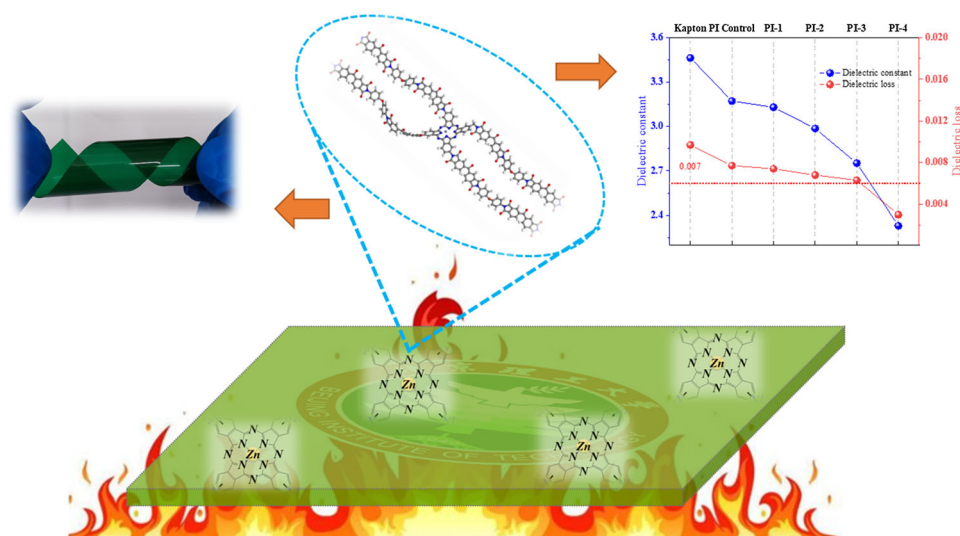
ABSTRACT

A series of novel tetraamino phthalocyanine zinc (TAPcZn) micro-crosslinked polyimide films were successfully synthesized by the copolymerization of 3,3',4,4'-benzophenone tetracarboxylic dianhydride and 4,4'-oxydianiline. The UV-Vis, FTIR, NMR, MALDI-TOF-MS, and SEM-EDS technologies were used to demonstrate the synthesis of TAPcZn. The copolyimide films were mainly characterized via their morphologies, thermal stability, and mechanical properties. As expected, the copolyimide films inherited the optical properties of phthalocyanine compounds and showed good mechanical properties, excellent thermal stability, and flame retardancy with low content of TAPcZn (< 5.0 wt%), regularly. Smooth, uniform, and defect-free copolyimide films all showed good mechanical properties, and the tensile strength of PI with 1.52 wt% of TAPcZn reached 116.9 MPa, which is 19.7% higher than that of pure PI. In addition, as the amount of TAPcZn increases, both the residue char and the initial decomposition temperature of the copolymer film improved significantly, and the fire resistance of PI showed the same rules according to the limiting oxygen index and UL-94 tests. Amazingly, the obtained copolyimides are π -conjugate macrocycle homogeneous copolymers with excellent low dielectric properties. In particular, the 4.49 wt% TAPcZn/PI film showed an ultra-low dielectric constant of 2.326 (at 1 MHz) and a dielectric loss of less than 0.007. Therefore, the copolyimide films containing TAPcZn are highly prospective candidates as high-performance flexible substrates and dielectrics for electronics devices.

Handling Editor: Gregory Rutledge.

Address correspondence to E-mail: hejiyu@bit.edu.cn

GRAPHICAL ABSTRACT



Introduction

Modified polymer films are composed of polymer matrix and dispersed particles such as nanofillers, metals, salts, and dyes [1–3]. Due to their combined properties of the matrix and dispersed substances, they are promising polymer candidates for optics, electronics, and sensors. More recently, polyimide (PI) films have been recognized as a class of mature electronic insulation commercially available polymeric materials for electronic packaging in the electronics, 5G communication, and aerospace industries [4–6]. PIs have many desirable characteristics such as high-temperature durability (service temperature can exceed 300 °C), excellent mechanical property, low dielectric constant, low relative permittivity, high breakdown voltage, inertness to solvent, and radiation resistance [7]. It is one of the most promising polymer candidates for the next generation of high-performance interlayer dielectrics.

With the advent of the 5G era, large-scale antenna arrays and highly integrated chips in aviation have put forward higher requirements for the PI's inherent performance, such as low dielectric (< 3.0), improved thermooxidative stability, and higher fireproof performance properties. To obtain higher thermal

stability and lower dielectric constants, various physical and chemical methods have been tried to alter the structure and properties of polyimide, such as surface modification [8], sol–gel and electrospinning techniques [9], and the introduction of functional groups into the PI chains [10]. For the molecular structure design of PI, the biggest challenge is to endow it with unique optical and electrical properties while balancing the PI film's thermal stability, and mechanical and dielectric properties.

Phthalocyanines, as a functional monomer of aromatic heterocyclic conjugated macrocycles with delocalized 18- π electron [11, 12], have been used in many application areas, such as organic thin-film transistors [13], chemical sensors [14], liquid crystals [15], photovoltaic cells [16], electrocatalysis [17], and photosensitizers in photodynamic therapy of cancer [18]. One of the most important assets of phthalocyanine molecules is their capability to coordinate with metal ions. Because the electron distribution in the metal-free phthalocyanine macrocyclic system is relatively uniform and the length of the C–N bond is almost equal, the diameter of the central hole is 0.27 nm, which can coordinate with almost all elements on the periodic table. The other attractive feature of phthalocyanine is its extremely high thermal and thermo-oxidative stability of its aromatic

character (15 times the benzene) [19]. It is well known that the initial decomposition temperature of the phthalocyanine ring is generally above 400 °C [20], which is a kind of functional material with high thermal stability. Recently, there has been a focus on combustion suppression using metallophthalocyanine (MPcs) chemistry [12, 21–23] with unique properties, particularly chemical and thermal stability. In addition, phthalocyanine rings are used to flame-retard thermoset resins, such as epoxy and benzoxazine resin [24]. Therefore, effectively combining phthalocyanine functional monomers with polyimide film materials, giving the film new special functions, and expanding the two application scenarios will certainly be a research work of potential significance and application value.

So far, rarely studies have explored the effects of metal phthalocyanines on the properties of PI copolymers. Among them, Achar et al. [19, 25, 26] systematically prepared a series of metal (Co/Ni/Cu) phthalocyanine polymerization and polyimide copolymers and focused on their heat resistance. Jung et al. [27] studied the application of PI film based on 4,4'-(hexafluoroisopropylidene) diphthalic and 4,4'-diaminodiphenyl anhydride (6FDA/ODA) copolymerized copper phthalocyanine (CuPc) in organic electroluminescent devices and found that the copolyimides containing Co and Cu-phthalocyanine exhibited better hole-transporting properties than doped-free PI. Maya [28] and Chen [21] investigated the optical and dielectric properties of high-content (50 wt%) CuPc polyimide copolymers. It is found that the CuPc-PI film shows good dielectric, thermal, and mechanical properties, making it a promising candidate for flexible dielectrics in modern microelectronics. However, previous studies mainly focused on the effect of Cu-, Ni-, and Co-containing phthalocyanines on the specific properties of copolymers, and the experimental studies on Zn-containing aminophthalocyanine and BTDA/ODA copolymerized PI films have not been systematically explored. Furthermore, all the above studies used high content of phthalocyanine (10–50 wt%), which can produce crystallization, phase separation or concentration gradients, especially the transmittance and roughness of thin-film samples limit its application to a certain extent. Therefore, its application is limited to a certain extent by a high concentration of insoluble phthalocyanines. It was also found that phthalocyanines exhibited remarkable dielectric properties [29, 30]

under aggregation and polymerization states due to 18 π -conjugated nitrogen heterocycles, mainly manifested in extremely low dielectric loss and dielectric response to maintaining good frequency stability. Of course, all the electrical and optical parameters depend on the central metal atom and the number, position, and presence of substituents [31].

The current work introduced rigid phthalocyanine zinc units into the molecular chains of BTDA/ODA via a novel synthesis of tetraamino phthalocyanine zinc (TAPcZn). To avoid extensive modification of the copolyimide properties, a limited number of phthalocyanine rings with low content of TAPcZn (less than 5 wt%) were introduced into the copolyimide. The effects of thermal, dielectric, optical, and flame retardant properties of micro-branched phthalocyanine units crosslinked PI films were investigated in detail.

Material and methods

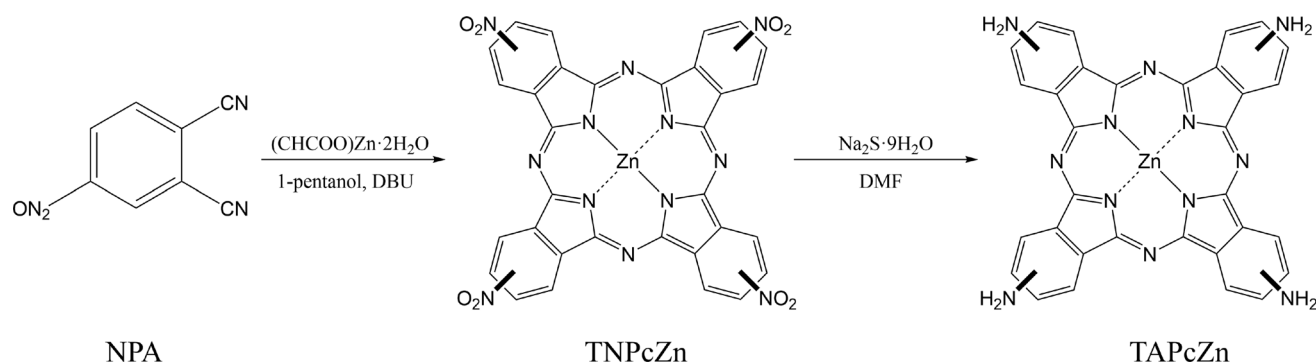
Materials

4-Nitrophthalonitrile (NPA) was purchased from Shanghai Macklin Biochemical Co., Ltd. 4,4'-oxydianiline (ODA, > 98%) and 3,3',4,4'-benzophenone tetracarboxylic dianhydride (BTDA, > 97%) were purchased from Shanghai Aladdin Biochemical Technology Co., Ltd. Zinc acetate dihydrate ($C_4H_6O_4Zn \cdot 2H_2O$, 99%), N-dimethylacetamide (DMAc, 99.8%, GC) and 1-pentanol (99.8%, GC) were purchased from Shanghai Macklin Biochemical Co., Ltd. BTDA was dried at 180 °C in vacuum for 24 h before use. N, N-dimethylformamide (DMF, 99.8%, GC, Aladdin) was purified by distillation under reduced pressure over calcium hydride and stored over 4 Å molecular sieves. Other solvents were obtained from various commercial sources and used without further purification.

Synthesis of tetraamino phthalocyanine zinc (TAPcZn)

Tetranitro phthalocyanine zinc (TNPcZn) and TAPcZn were synthesized in our laboratory from NPA by a method detailed in a reported procedure [32] shown in Scheme 1.

In a 250-ml flask, NPA (5.19 g, 30 mmol), zinc (II) acetate (2.20 g, 10 mmol), and DBU (6.08 g, 40 mmol)



Scheme 1 Synthetic routes of TNPcZn and TAPcZn.

were stirred in dried n-pentanol at 142 °C for 24 h under argon. After cooling to room temperature, the mixture was filtered and washed with methanol and ethanol. The dark green solid product TNPcZn was obtained with a yield of 80.2%. Then, TNPcZn (1.514 g, 2 mmol) and Na₂S·9H₂O (5.76 g, 24 mmol) were stirred in dried DMF at 65 °C for 4 h under argon. After cooling to room temperature, the mixture was filtered and washed with methanol, ethanol, and deionized water. TNPcZn was obtained in a 50.7% yield. An isomeric mixture of the desired TAPcZn was synthesized as expected. Anal. calcd for TAPcZn: C, 50.0; H, 4.16; N, 9.71. Found: C, 48.9; H, 4.38; N, 9.31. HR MALDI-TOF MS for C₃₂H₁₆N₁₂O₈Zn (calcd. 636.1225): *m/z* = 636.2150.

Preparation of PI/TAPcZn copolyimide films

The compositions of the PI/TAPcZn copolymer samples are listed in Table 1. In formulating PI/TAPcZn copolyimides, the molar ratio of -NH₂ in TAPcZn and ODA was equal to the anhydride

groups in BTDA. The solid contents of all the solutions in Table 1 were 10 wt%.

The PI/TAPcZn copolyimides were prepared by the procedure depicted in Fig. 1. The specific preparation process is roughly described as follows: A three-neck flask was first purged with nitrogen gas in a cold-water bath to remove moisture. Then, DMAc (50 mL) was added, and a gentle stream of nitrogen was passed through the solution. ODA was introduced into the flask under stirring. BTDA was then added in five portions and then the TAPcZn. Until dissolved completely, a clear BTDA/ODA/TAPcZn/DMAc solution was obtained. The mixture was stirred under N₂ at 10 °C for 24 h to form a viscous and homogeneous polyamic acid (PAA) precursor solution. The PAA solution was then cast horizontally on a clean glass substrate in a vacuum oven to remove bubbles for 4 h at 60 °C. The xerogel film was heated sequentially at 80 °C for 12 h, 120 °C for 4 h, 200 °C for 1 h, 250 °C for 1 h, and 350 °C for 1 h with the same heating rate of 2–3 °C min⁻¹ in a drying oven. After cooling to room temperature, a flexible PI/TAPcZn composite film was self-stripped from the

Table 1 Compositions of PI/TAPCZN copolyimide films

Materials	PI-Control PI/TAPcZn/0	PI-1 PI/TAPcZn/0.5	PI-2 PI/TAPcZn/2.5	PI-2' ^a PI/PcZn/2.5	PI-3 PI/TAPcZn/5.0	PI-4 PI/TAPcZn/7.5
BTDA (g)	3.084	3.080	3.066	3.037	3.049	3.032
ODA (g)	1.916	1.905	1.858	1.887	1.800	1.743
TAPcZn (g)	0	0.015	0.076	0.076	0.150	0.224
n(-NH ₂ in TAPcZn)/n(-NH ₂)	0	0.5%	2.5%	0	5.0%	7.5%
TAPcZn ^b (wt%)	0	0.30	1.52	1.52	3.01	4.49
DMAc (mL)	50	50	50	50	50	50

^aNon-amino PcZn as a substituent of TAPcZn in PI-2' was mixed in PAA solution with the same solid content (2.5 wt%); ^bThe mass fraction is calculated by the molar ratio of -NH₂ in TAPcZn

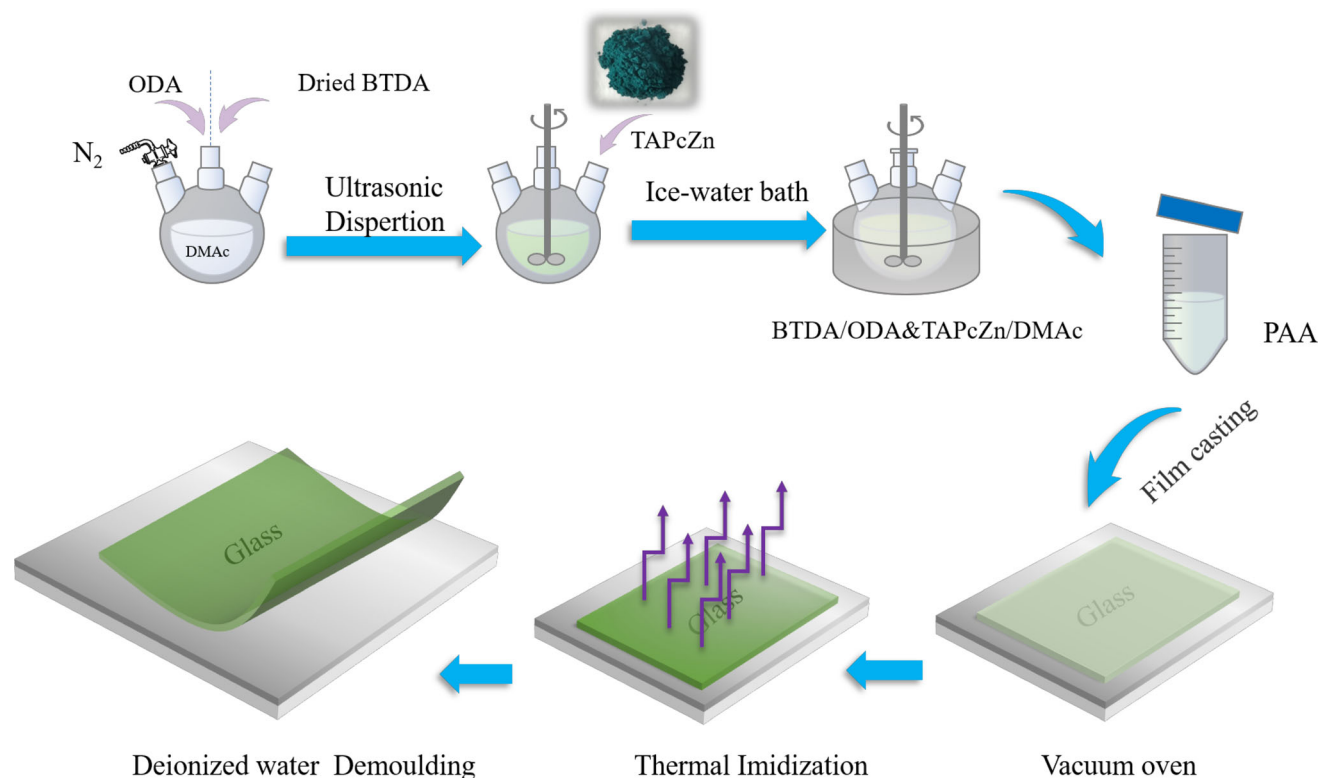


Figure 1 The processing method of copolyimide films.

glass surface by soaking in deionized water. After cleaning (ultrasonic cleaning with ethanol, acetone and deionized water and blowing dry with nitrogen), we obtained all the neat and lucent PI films with a thickness of approximately 50 μm . The synthesis route and suggested chemical structure of PI/TAPcZn materials are shown in Fig. 2.

Characterization

FTIR spectra were recorded on a Nicolet 6700 IR spectrometer at 4 cm^{-1} with a full reflectance mode of 32 scans. ^1H NMR was recorded on a Bruker Avance 600 NMR spectrometer operating in Fourier transform mode. Ultraviolet–visible (UV–Vis) spectroscopy was measured using a Mettler-Toledo UV7 spectrometer. Element analysis of C, O, and N was carried out using a Vario EL Cube elemental analyzer. MALDI-TOF MS was performed with a Bruker Autoflex III device. It was equipped with a pulsed nitrogen laser ($\lambda = 337\text{ nm}$, pulse width = 3 ns, and average power = 5 mW at 20 Hz). The extraction voltage in the TOF analyzer was 20 kV, and ions were obtained by irradiation just above the threshold laser power. Thermogravimetric analysis (TGA) was

performed using a thermal analyzer (Netzsch 209 F1) under a nitrogen flow rate, with a heating rate of $10\text{ }^\circ\text{C min}^{-1}$ from 40 to $800\text{ }^\circ\text{C}$. Differential scanning calorimetry (DSC) measurements were taken on a Netzsch DSC 204 F1 instrument in the temperature range of $30\text{--}350\text{ }^\circ\text{C}$ with a heating rate of $10\text{ }^\circ\text{C/min}$ in a nitrogen flow of 20 mL min^{-1} . Dynamic mechanical analysis (DMA) of the films was performed using a Mettler Instrument DMA/SDTA861e at a heating rate of 2 K min^{-1} and a frequency of 2 Hz. The coefficient of thermal expansion (CTE) of the PI films was measured by the dilatometer (DIL 402, Netzsch). The temperature range was $25\text{--}200\text{ }^\circ\text{C}$ with a rate of $5\text{ }^\circ\text{C min}^{-1}$. Morphology characterization of the phthalocyanine particles, char residue, and film was performed with a Hitachi SU8020 scanning electron microscope (SEM) sputtering the surface with Au under a high vacuum with a voltage of 15 kV and a Hitachi HT7700 transmission electron microscopy (TEM) via a 120 kV electronic source. The C, O, N, and Zn elements in the residue were verified by an energy-dispersive X-ray spectrometer (EDXS EX-350) under SEM. Atomic force microscopy (AFM) pictures of the specimens were collected via a Bruker Dimension Icon SPM in the tapping mode in air,

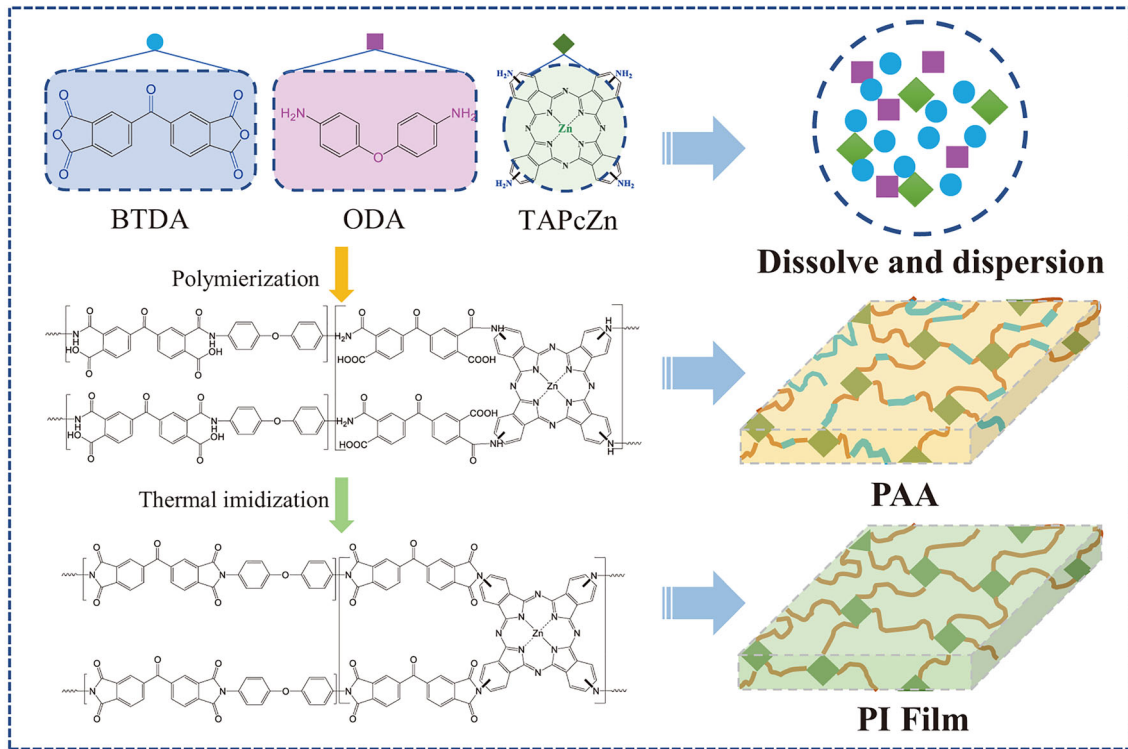


Figure 2 Synthetic Scheme of copolyimide films.

ScanAsyst Air probe, $k = 0.4 \text{ N m}^{-1}$, and $f_0 = 70 \text{ kHz}$. X-ray diffraction (XRD) analysis was achieved using an XPERTPRP diffractometer system; Cu K α radiation was used with a copper target over the 2θ range of $5\text{--}60^\circ$. The mechanical property was tested using a universal machine (CMT-410 4, MTS Systems (China) Co., Ltd.). The dimensions of the samples were $150 \times 10 \text{ mm}^2$ according to ASTM D882-91, and the results are the average of five measurements. The dielectric properties of the PI films sputtered the surface with Ag were evaluated by an Agilent 4294A over the frequency range of $40\text{--}110 \text{ MHz}$ and a TongHui TH2826 LCR Meter High Frequency (at 10 GHz) with the same test fixture (TongHui TH26008A). The limiting oxygen index (LOI) was obtained by an oxygen index analyzer (TESTech Instrument Technologies Co., Ltd. Suzhou, China) according to ASTM D2863 by measuring the minimum oxygen concentration required to support the candle-like combustion of films. The rolled film was obtained by winding the film with the dimensions of $160 \times 20 \text{ mm}^2$ at a 45° angle on a diameter of 2 mm barrel. The UL-94 Vertical burning tests were performed on a CZF-5A-type instrument (Jiangning Analysis Instrument Company, China)

with specimen dimensions of $150 \times 15 \text{ mm}^2$ according to the ASTM D3801.

Results and discussion

The characterization of synthesized TAPcZn

In addition, the chemical structure of the TAPcZn elaborated by FTIR, $^1\text{H NMR}$, and UV-Vis spectra is shown in Fig. 3a–d. The absorption peaks at 1132 , 1076 , 1045 , 842 , 755 , and 725 cm^{-1} were assigned to the phthalocyanine skeleton [32], and the band around 3300 cm^{-1} corresponded to the $-\text{NH}_2$ group. To further confirm the structure of TAPcZn, $^1\text{H NMR}$ was employed to characterize the products displayed in Fig. 3b. The peaks between 7.0 and 9.0 ppm were assigned to the aromatic protons (labeled a, c and d) for the benzene ring. In comparison, the peak area at 6.45 ppm assigned to the hydrogen on the benzene amino group was twice the area of a, c, or d peaks.

The structures of TNPcZn and TAPcZn were further confirmed by UV-Vis. The linear optical properties of PI films were studied in terms of absorption measurements in the UV-Vis region ($200\text{--}1000 \text{ nm}$).

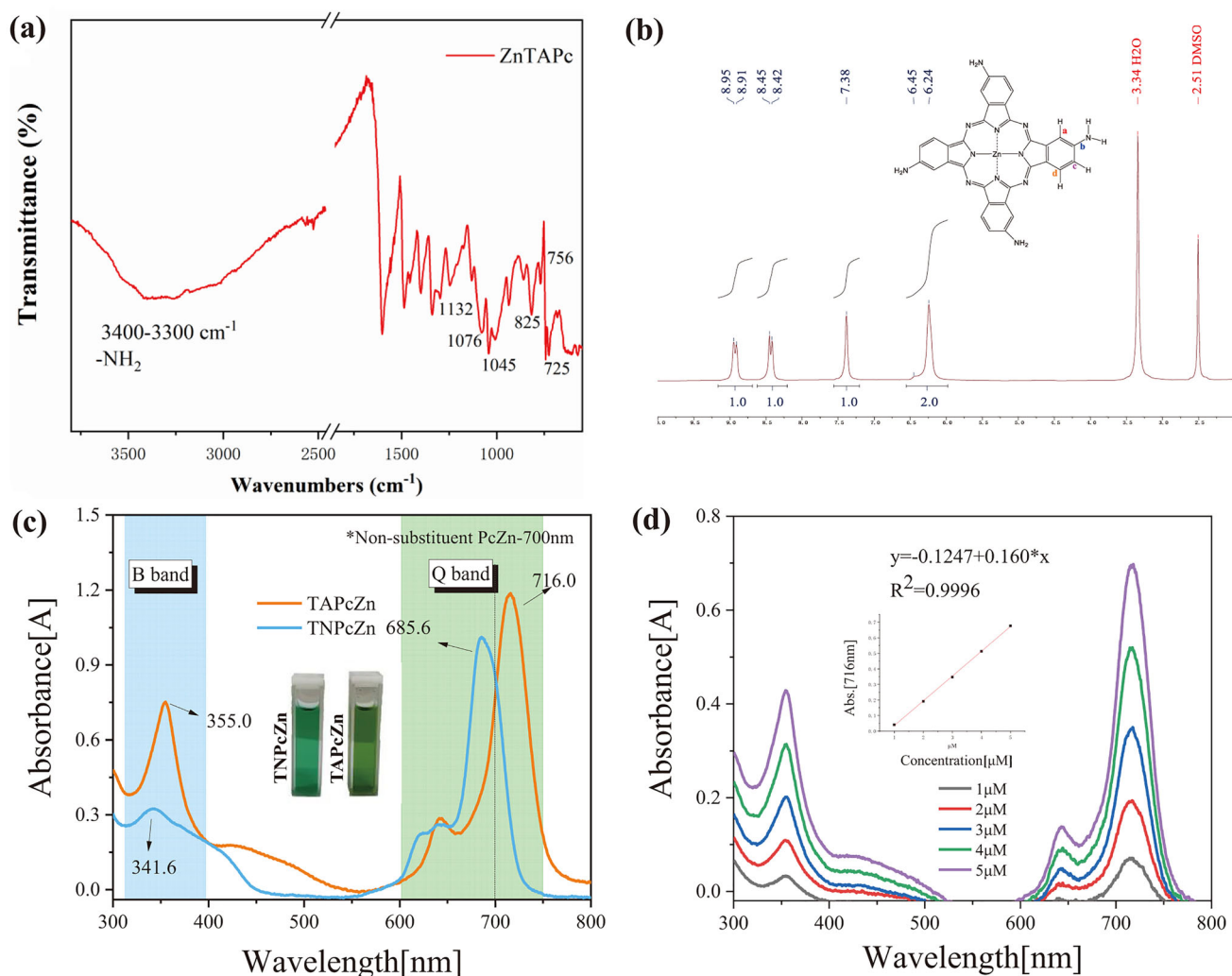


Figure 3 The characterization of synthesized TAPcZn. **a** FTIR and **b** ^1H NMR spectra of TAPcZn; UV-Vis spectra of **c** TAPcZn and TNPcZn in DMF, and **d** TAPcZn at various concentrations (from 1.0 to 5.0 μM) in DMF.

Absorption bands at wavelengths shorter than 270 nm were not considered because of the cutoff point of the solvent (DMF 270 nm) [33]. In general, there are two characteristic peaks in the phthalocyanines: one absorption peak in the UV region (300–400 nm), which is known as the Soret (*B*) band, and another broad absorption peak in the visible region (650–750 nm), which is known as the *Q* band. The *B* band and *Q* band are attributed to the $n-\pi^*$ transition and $\pi-\pi^*$ transition on phthalocyanine, respectively [34, 35]. As shown in Fig. 3a, two typical peaks of *B* and *Q* bands are observed in TNPcZn and TAPcZn. Moreover, for TAPcZn, the redshift of the *Q* band caused by the electron-donating ability of the amino group is also confirmed. In addition, another peak appears at 640–650 nm, which corresponds to

the absorption of TAPcZn vibronic dimer [36]. The aggregation behavior of the TAPcZn at different concentrations of DMF was studied (Fig. 3b). The absorption of the *Q* band increased proportionally with the concentration of the TAPcZn, and no new bands that could be attributed to the aggregated forms were found [37]. The UV-vis absorption intensity and TAPcZn concentration obeyed Beer-Lambert law at concentrations below $5 \times 10^{-5} \mu\text{M}$, and their relationship was under a linear optical property. From the above analysis, it could be confirmed that the target product TAPcZn was synthesized successfully.

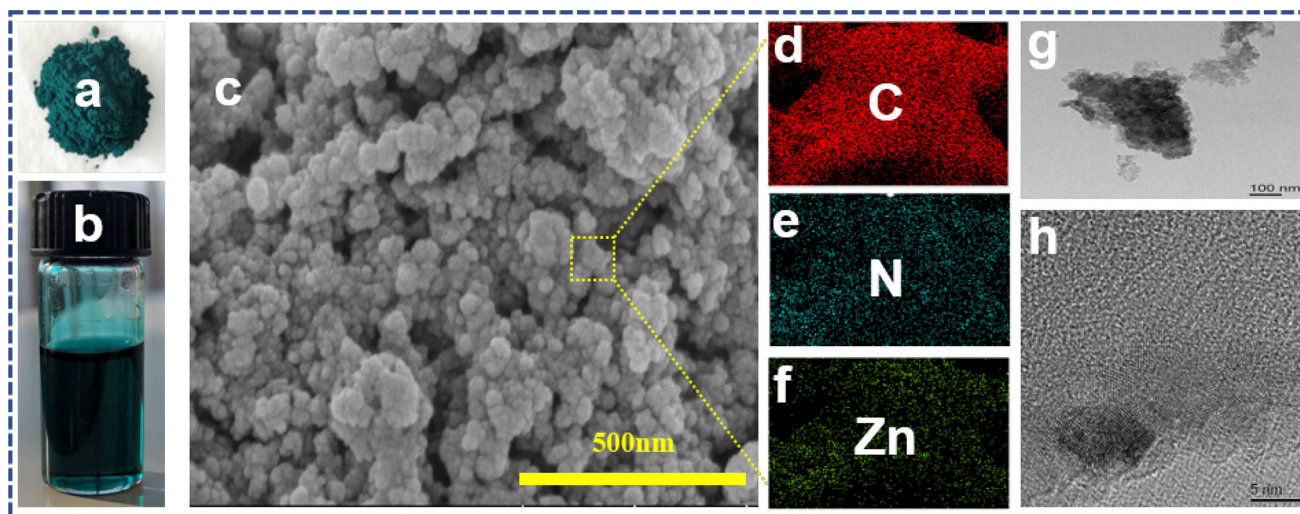


Figure 4 Morphology of the synthesized TAPcZn. Photographs of the TAPcZn powders **a** and their dispersion in DMAc forming a homogeneous suspension **b**, SEM image of the TAPcZn powders

Morphology characterization of the synthesized TAPcZn

Figure 4 shows the morphology characterization of TAPcZn powders. The obtained dark green powders (Fig. 4a) can be homogeneously dispersed in DMAc (Fig. 4b). Figure 4c shows representational SEM images of the TAPcZn powder. It can be seen that the powder surface is rough and that the typical particle size is less than 100 nm. The elemental mappings show Zn elements homogeneously dispersing over the whole particle (Fig. 4f). As shown in Fig. 4g, one particle demonstrates that the few-stacked nanostructure was obtained. Partial lattice fringes belonging to TAPcZn were monitored by high-magnification TEM (Fig. 4h), which can be speculated that the powder is in the form of coexistence of crystalline and amorphous states.

The FTIR Spectrum of PAAs and PI Films

The FTIR spectrum of PAAs showed bands at 1721 cm^{-1} (carboxyl) and 1660 cm^{-1} (imide) owing to C=O stretching and at 1550 cm^{-1} owing to C–N stretching (imide), suggesting the formation of PAA [38] (Fig. 5c). According to Fig. 5d, all the characteristic absorption peaks of PI incorporating TAPcZn segments were well designated in the FTIR curves of the PAAs and films. Strong bands at 1776 cm^{-1} ($\nu_{\text{asym}}\text{ C=O}$), 1708 cm^{-1} ($\nu_{\text{sym}}\text{ C=O}$), 1363 cm^{-1} ($\nu_{\text{CN}}\text{ imide}$), and 725 cm^{-1} (imide ring deformation vibrations)

c, and EDS elemental mapping images of C, N, and Zn **d–f**, high-magnification TEM **g**, **h** images of TAPcZn powders.

belonged to imide rings of imide ring. In addition, no absorption bands were observed for the anhydride (1854 cm^{-1}) and the free $-\text{NH}_2$ ($3300\text{--}3500\text{ cm}^{-1}$), indicating that the monomer reaction is complete. The C–N bending vibration peaks of TAPcZn overlapped with the characteristic peaks of PI/TAPcZn films. Consequently, the PI film with TAPcZn segments was prepared successfully.

Morphological properties of polyimide films

AFM was used to observe the microscopic surface morphology of copolyimide films. Generally, the arithmetic means deviation R_a and the root mean square roughness R_q are used to characterize the roughness of the sample, and the larger the R_a , R_q , the greater the roughness. The 3D image of the PI-control, PI-1 and PI-2 (Fig. 6a) showed that the films only have few protrusions, no noticeable depressions, and the overall performance is flat. As shown in Fig. 6b, the PI-control, PI-2, and PI-4 were found to have image R_q values of 1.020 nm, 1.268 nm and 1.228 nm of and R_a values of 0.749 nm, 0.852 nm, and 0.816 nm, respectively, demonstrating the roughness of copolyimide films are relatively low and overall flat. Differently, the PI-2' film prepared by physical mixing showed greater image roughness ($R_a = 1.393\text{ nm}$ and $R_q = 2.086$). Furthermore, the surface morphology of the PI/TAPcZn films was checked by SEM as well, which is illustrated in Fig. 6c. It was found that the surface of the PI control, PI-2, and PI-4

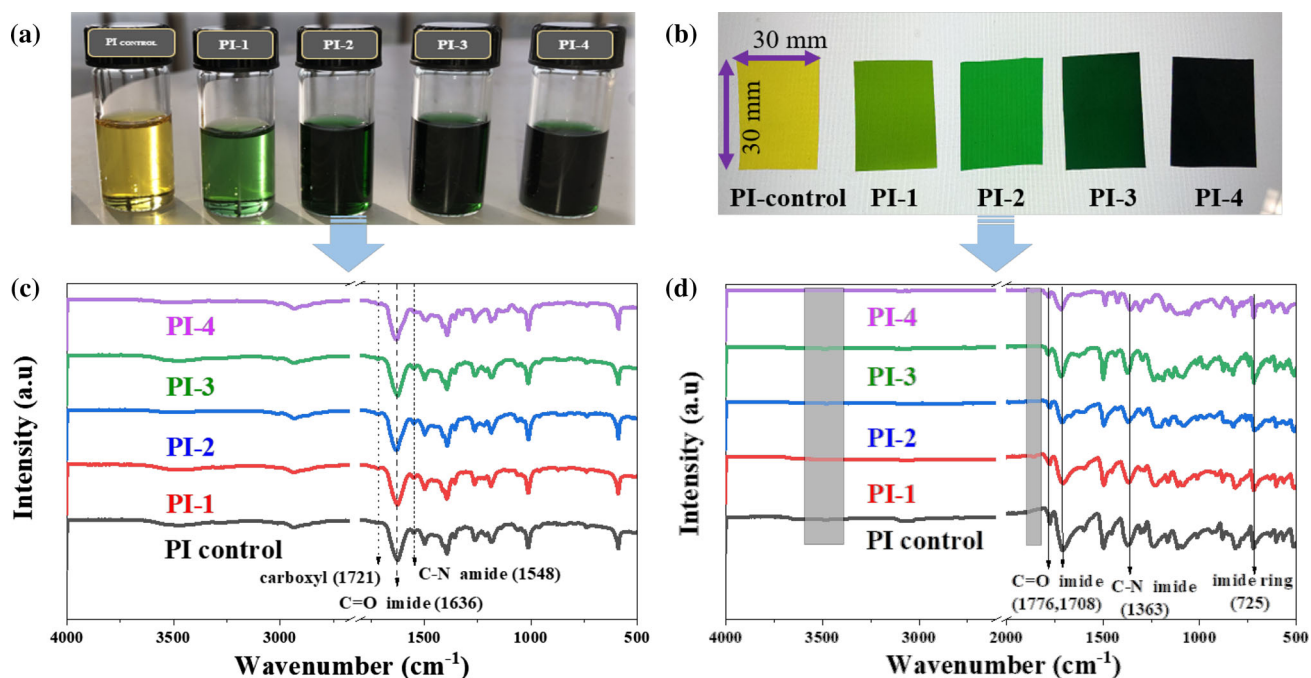


Figure 5 The photograph of PAA **a** and PI film copolyimides **b**, and the FTIR spectra of PAA **c** and PI film copolyimides **d**.

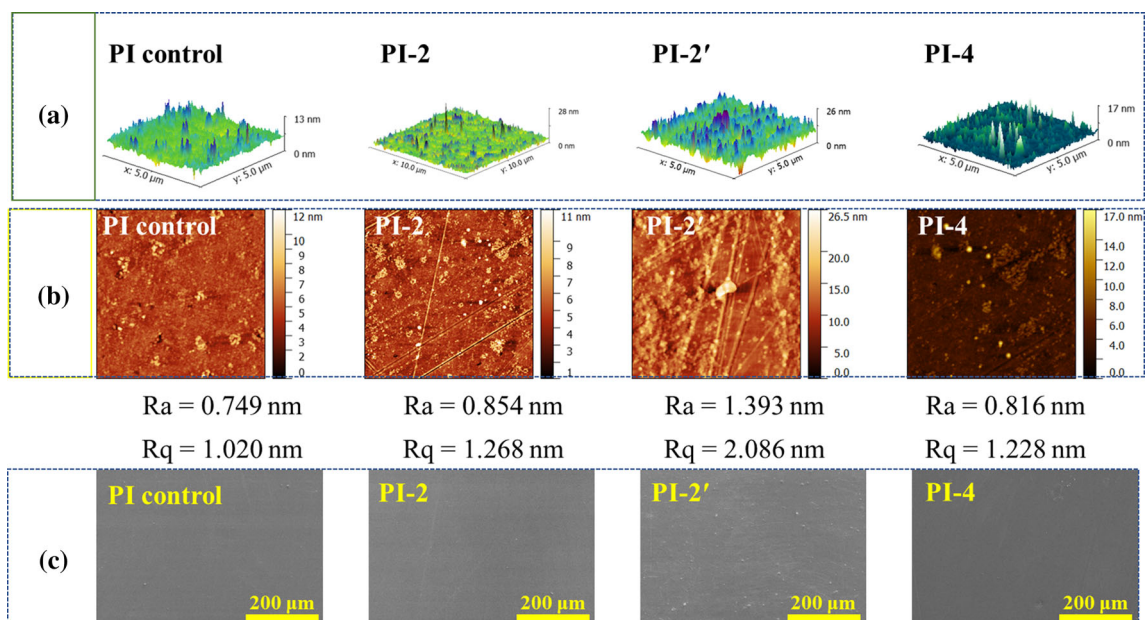


Figure 6 Morphological properties of typical films, PI control, PI-2, and PI-4 films: **a** AFM 3D view, **b** AFM height images ($5 \mu\text{m} \times 5 \mu\text{m}$) with roughness parameter (R_a and R_q), and **c** SEM images.

was flat, clean, and had no obvious defects under the electron microscope at a magnification of 50 times. However, for PI-2', some white bumps appeared on the surface, which was consistent with the test results of AFM. It was speculated that it was caused by the

agglomeration of TAPc in the PI system. PI-2' samples will not be considered in the follow-up study.

Thermal properties

Good heat resistance is also one of the most important property requirements for the applications of PI

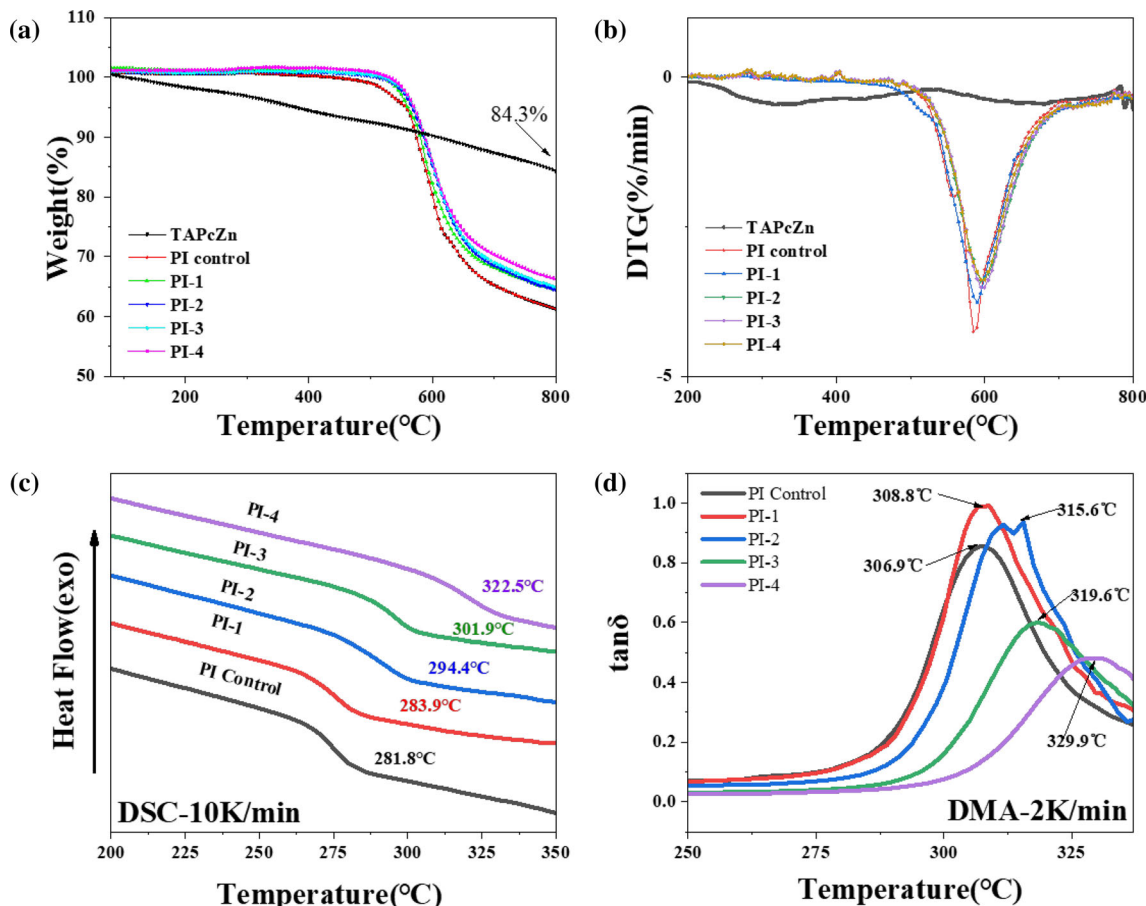


Figure 7 a TG, b DTG, c DSC, and d DMA curves of TAPcZn, PI control, and PI/TAPcZn films.

films. Figure 7 shows the glass transition temperatures (T_g) of the PI/TAPcZn films, which were characterized using DSC and DMA. The DSC results (Fig. 7d) revealed that PI films exhibited an extremely higher T_g with the TAPcZn load, and the maximum value was up to 322.5 °C (PI-4). DMA was also adopted to evaluate the T_g , and the results are illustrated in Fig. 7c. As expected, the variation in T_g measured by DMA showed a similar trend compared with the DSC results. The plots of loss factor $\tan \delta$ (Fig. 7c) display only one relaxation process, corresponding to the glass transitions of the copolyimides with different TAPcZn loadings, which further demonstrates the homogeneous dispersion of the TAPcZn additive in the PI matrix. The loss factor $\tan \delta$ of PI/TAPcZn films showed higher values than that of the PI control film in the temperature range from 40 to 380 °C, attributed to the crosslinking effect on the matrix. The width of the $\tan \delta$ curve at T_g indicated the synergistic effect of polymer molecular chains during material relaxation, which was related

to the relaxation of polymer molecular chains that usually caused the broadening $\tan \delta$ peak due to the restricted chain movement [5]. All the PI films maintained good heat resistance, with the T_g values of the PI films increasing in the order of PI control < PI-1 < PI-2 < PI-3 < PI-4. The introduction of phthalocyanine rings increased the heat resistance of the PI/TAPcZn films. These results also indicated that the π -conjugate macrocycle of TAPcZn limits the mobility of the PI chains in the crosslinking network.

Moreover, none of the films showed clear melting endothermic peaks up to the decomposition temperatures on their DSC thermograms, which demonstrated the amorphous nature of these PI films based on the rigid coplanar conjugated phthalocyanine ring. The thermal stabilities of the PI/TAPcZn films were evaluated by TGA, as shown in Fig. 7a, b. The relevant thermal decomposition data, including the T_{onset} , defined as the temperature at 5% weight loss, the T_{max} , defined as the temperature at the

Table 2 Thermal data of PI/TAPcZn films

Samples	CTE (ppm/K)	T _{onset} (°C)	T _{max} (°C)	Residue at 800 °C (%)
PI control	54.90	557.6	587.3	61.42
PI-1	49.12	565.8	589.5	63.70
PI-2	45.80	567.0	595.1	64.42
PI-3	42.64	569.5	597.7	64.94
PI-4	40.10	570.2	597.2	66.23

maximum weight loss rate, and the char residues at 800 °C, are given in Table 2.

According to Fig. 7b, pure nano-grade TAPcZn powders show excellent thermal stability (no obvious decomposition) and a high char residue (84.3%) at 800 °C under N₂ atmosphere. All the PI films exhibited good thermal stability before 500 °C in nitrogen. Moreover, TAPcZn loading did not change the PI degradation path, and the thermogravimetric behaviors of the PI/TAPcZn films were similar to that of the PI control. Compared to the PI control, the PI/TAPcZn exhibited slightly higher residue that increased with the TAPcZn load. It has been reported that the presence of some TAPcZn as a synergist could increase char yields [39]. These results indicate that the interaction between TAPcZn and PI produces a high char yield.

As shown in Table 2, the CTE of PI control decreased from 54.9 to 49.12 ppm/K after adding 0.30 wt% TAPcZn (PI-1). It decreased from 49.12 to 40.10 ppm/K as the concentration of TAPcZn. It is well known that the chemical structure, morphology, and orientation of the molecular chain determine the CTE of the polymer. In general, introducing a rigid structure into the main chain to inhibit the orientation of the chain can often reduce the CTE value. In this work, the decrease of the CTE could be attributed to the expansion or contraction of the PI matrix restrained effectively by the 3D crosslinked network structures between TAPcZn containing rigid phthalocyanine rings and PI [40].

Table 3 mechanical properties of PI/TAPcZn films

Samples	Tensile strength (MPa)	Young's modulus (GPa)	Elongation at break (%)
PI control	97.7 ± 3.4	2.06 ± 0.09	7.1 ± 0.4
PI-1	98.2 ± 1.1	2.00 ± 0.07	7.2 ± 0.4
PI-2	116.9 ± 2.1	2.05 ± 0.08	8.5 ± 0.8
PI-3	105.5 ± 3.3	2.17 ± 0.08	6.2 ± 0.8
PI-4	94.4 ± 4.3	2.35 ± 0.03	4.7 ± 1.0

Mechanical properties

The effects of TAPcZn content on the mechanical properties of the PI/TAPcZn were studied. The tensile strength, elongation at break, and Young's modulus of the PI/TAPcZn are shown in Table 3. The tensile strengths and tensile moduli of the films were in the range of 94–116 MPa and 2.06–2.35 GPa, respectively. Such improvement was possibly contributed by the restriction and effect of the introduction of rigid ring structures and the formation of micro-crosslinked systems on the polymer chains. When the amine group concentration of TAPcZn was 2.5% (PI-1), the tensile strength at break increased from 97.7 to 116.9 MPa. However, the tensile strength of PI films declined with increasing TAPcZn content. For example, the tensile strength of PI-4 was only 94.4 MPa. Thus, a small amount (≤ 3.01 wt%) of the crosslinked rigid structures of TAPcZn clusters could enhance the tensile strength of PI films. Moreover, the improvement in Young's modulus and the decrease in elongation at break could be possibly contributed by the synergistic effects of rigid phthalocyanine ring and inter-molecular connection due to TAPcZn incorporation. Overall, the PI-2 sample film showed optimal mechanical performance. A small amount of TAPcZn can overcome the disadvantages of reduced mechanical properties and high costs due to dependence on large amounts of modified materials.

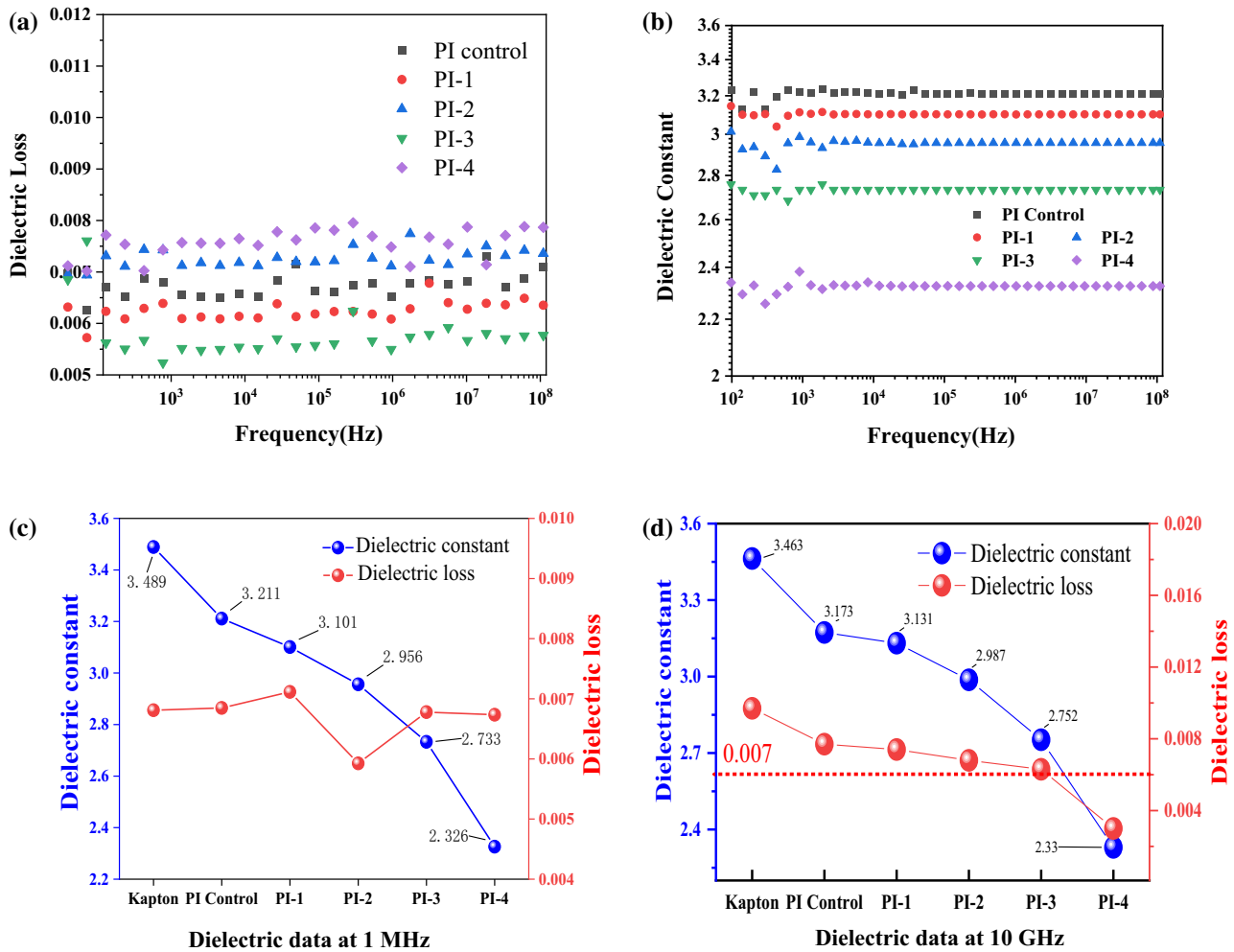


Figure 8 Dielectric properties of the PI/TAPcZn films: dielectric constant **a**, dielectric loss **b**, dielectric constant, and dielectric loss at 1 MHz **c**, and dielectric constant and dielectric loss at 10 GHz **d**.

Dielectric properties

As one kind of electrical insulating material, PIs are widely used in the electronics industry and require a low dielectric constant. Figure 8a, b shows the dielectric and dielectric loss tangent-frequency curves of pure PI films and PI films with different contents of TAPcZn, respectively. The four PI/TAPcZn films had good frequency stability, and their dielectric constants hardly changed in the frequency range of 50–10⁸ Hz.

The dielectric constants of all the films at 1 MHz are summarized in Fig. 8c to reveal the influence of TAPcZn content. Additionally, compared with the commercial DuPont Kapton films (dielectric constant of 3.489) and PI control film (dielectric constant of 3.211), the PI/TAPcZn films provided a substantially lower dielectric constant and smaller dielectric loss

with the increasing TAPcZn. Consequently, the optimum dielectric constant reached 2.326 (PI-4 at 1 MHz), and the dielectric loss was still 0.007. Generally, the reduction of the dielectric constant and dielectric loss are usually achieved by polymer molecular structure design. Low polarizability chemical bonds, asymmetric, rigid non-planar conjugated structures or flexible structures, and space-occupying groups were added to the dielectric material to increase the free volume in the polymer structure [41]. Thus, the actual dielectric constant decline in PI/TAPcZn films was quite unusual and unexpected. However, A small amount of TAPcZn was introduced into the conjugated plane of PI molecules as a crosslinking point to form micro-branched crosslinked structures. The micro-cross-linked structure firstly destroyed the original arrangement of PI chains regionally, increased the

spacing of some molecular chains, destroyed the order of molecular chains, inhibited the polarization and relaxation of polar molecular groups, thus increasing the FFV of the system. It is undeniable that this micro-branched crosslinking also promotes tight packing of molecular chains, but studies have shown that at low content levels, the effect of this promotion is weaker than the former [42], resulting in the lower dielectric constant of PI films and stable dielectric loss.

In general, the dielectric constant of PI films is known to decrease gradually with increasing frequency [1, 43, 44]. However, at ultrahigh frequencies, the dielectric constant of the actual test results for PI/TAPcZn remained roughly constant. In contrast, the dielectric loss gradually decreased at 10 GHz (Fig. 8d). This is significant for the specific application of low dielectric materials in microelectronics and 5G communication [45].

Flame retardancy properties

As electronic packaging and insulation materials, stable heat resistance and non-flammable PI films are necessary. The LOI and vertical burning classifications (UL-94) are frequently used to characterize fire retardancy. The LOI represents the minimum oxygen level in the atmosphere to sustain flames on a polymer material [46]. The higher the LOI value, the higher the non-flammability. The LOI values of PI films effectively increased with the increasing TAPcZn (Fig. 9a). When 1.51wt% TAPcZn was incorporated, the LOI value of PI-2 increased from 47.5% of PI control to 52.4%, and the LOI of PI-4 with 4.49wt% TAPcZn increased by 11.8% (LOI = 53.1%).

Table 4 Flame retardant properties of PI films

Sample	After flame times		Dripping	UL-94 VTM	LOI
	t_1 (s)	t_2 (s)			
PI control	4	2	No	VTM-0	47.5
PI-1	4	1	No	VTM-0	49.6
PI-2	3	1	No	VTM-0	52.4
PI-3	3	1	No	VTM-0	52.6
PI-4	2	1	No	VTM-0	53.1

Furthermore, all the PI films were classified as UL-94 VTM-0 (Table 4). After flame times for all individual PI films did not exceed 5 s, no dripping was observed. Generally, the char residue is used to analyze the solid phase flame retardancy mechanism of combustion [47]. SEM images of the PI control and PI-4 after combustion at oxygen concentrations of 47.5% and 53.1% are illustrated in Fig. 9c–f. The surface morphology of the char could be significant for solid-phase flame retardancy. Compared to the PI control, the outer surface of PI/ZnTAPc formed a dense layer of fish scale-like residue (Fig. 9d), preventing heat flow and mass transport. The EDX spectrum of PI-4's exterior char residue showed the C, O, and Zn elements of TAPcZn, indicating the existence of TAPcZn in the matrix and Zn in promoting char formation. The internal char layer structure is smooth and flat (f) and is not decomposed by flame erosion.

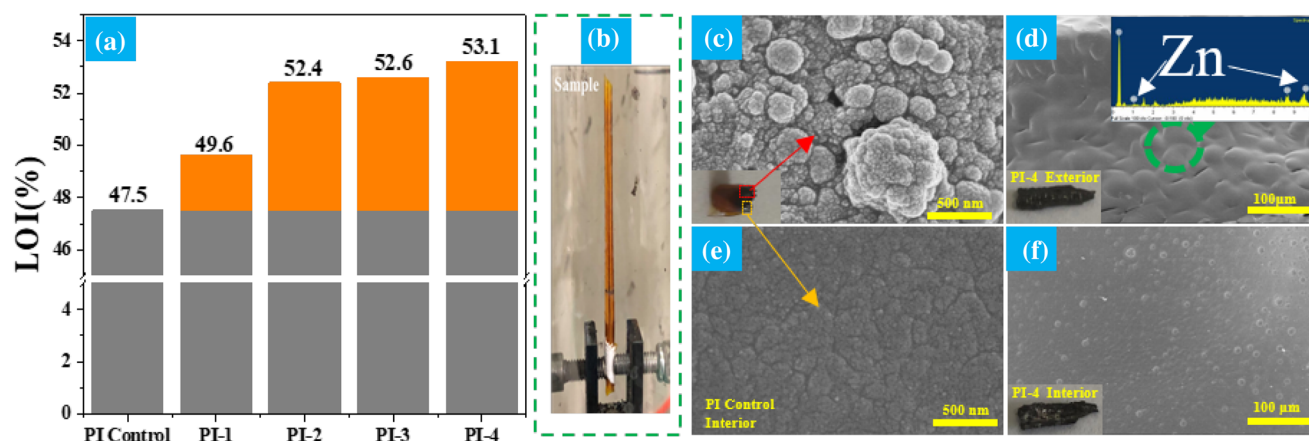


Figure 9 LOI test of PI films. **a** Histogram of LOI values, **b** sample photo of the LOI test, and **c–f** SEM images of the exterior and interior char residues of PI control and PI-4 after combustion at oxygen concentrations of 47.5% and 53.1%, respectively.

Conclusions

In summary, a series of novel PI/TAPcZn films were prepared via copolymerization and subsequent thermal imidization. FTIR, ^1H NMR, and UV–Vis confirmed that the TAPcZn was successfully prepared. The PI/TAPcZn films exhibited preferable thermal stability, mechanical performance, dielectric properties, and flame retardant, contributing to the development of polymer substrates with low dielectric constants, unique thermal requirements, and excellent overall performance. According to the AFM and SEM images, it could conclude that the TAPcZn showed better nano-level dispersibility and compatibility with the PI matrix than the TNPcZn, which brought about better overall performance. Compared with PI control, the T_g and char residue of the PI/TAPcZn films increased while the CTE values decreased with the increase of TAPcZn content, resulting in excellent heat resistance. In addition, a certain amount of Rigid TAPcZn can significantly improve the mechanical strength and modulus. Besides, we found that the dielectric loss and dielectric constant of PI/TAPcZn films were significantly reduced due to microbranching effect attributed to a stronger enlarging molecular interlayer and enlarging system FFV than crosslinking-limited, and the optimum dielectric constant reached 2.326 (at 1 MHz). Finally, while the UL-94 test maintained the V-0 rating, the LOI of PI/TAPcZn was markedly improved with increasing TAPcZn content, showing outstanding flame retardant performance.

Therefore, this research indicated that the PI films with TAPcZn had a broad prospect because of low filler content while high performance. It is strongly believed that the good comprehensive properties make functional PI/TAPcZn films good candidates, as flexible insulating layers can open up a vast array of applications in the microelectronics, 5G communication, and aerospace industries.

Acknowledgements

This research did not receive any specific grant from funding agencies in the public, commercial, or not-for-profit sectors.

Author contributions

YZ was involved in the validation, methodology, investigation, writing—original draft preparation. JH contributed to the supervision, writing—review and editing. RY contributed to supervision and project administration.

Declarations

Conflict of interest Conflict of interest the authors declare that they have no conflict of interest.

Supplementary Information: The online version contains supplementary material available at <http://doi.org/10.1007/s10853-022-07641-7>.

References

- [1] Chen Z, Tong F, Zhu D, Lu X, Lu Q (2019) Ductile polyimide/reduced graphene oxide nanohybrid films with porous structure fabricated by a green hydrogel strategy. *ACS Appl Polym Mater* 1:914. <https://doi.org/10.1021/acsapm.9b00234>
- [2] Ou X, Chen S, Lu X, Lu Q (2021) Enhancement of thermal conductivity and dimensional stability of polyimide/boron nitride films through mechanochemistry. *Compos Commun* 23:100549. <https://doi.org/10.1016/j.coco.2020.100549>
- [3] Nie P, Min C, Song HJ, Chen X, Zhang Z, Zhao K (2015) Preparation and tribological properties of polyimide/carboxyl-functionalized multi-walled carbon nanotube nanocomposite films under seawater lubrication. *Tribol Lett* 58:1. <https://doi.org/10.1007/s11249-015-0476-7>
- [4] Liu R, Wang K, Liu Z et al (2021) In situ growth of silver film on polyimide with tuned morphologies for flexible electronics. *Langmuir* 37:9540. <https://doi.org/10.1021/acs.langmuir.1c01392>
- [5] Liu Y, Qian C, Qu L et al (2015) A bulk dielectric polymer film with intrinsic ultralow dielectric constant and outstanding comprehensive properties. *Chem Mater* 27:6543. <https://doi.org/10.1021/acs.chemmater.5b01798>
- [6] An L, Yang Z, Zeng X et al (2022) Flexible and quasi-isotropically thermoconductive polyimide films by guided assembly of boron nitride nanoplate/boron nitride flakes for microelectronic application. *Chem Eng J*. <https://doi.org/10.1016/j.cej.2021.133740>
- [7] Leu C-M, Reddy GM, Wei K-H, Shu C-F (2003) Synthesis and dielectric properties of polyimide-chain-end tethered

- polyhedral oligomeric silsesquioxane nanocomposites. *Chem Mater* 15:2261. <https://doi.org/10.1021/cm0208408>
- [8] Zhang Y, Li Y, Li G et al (2007) Polyimide-surface-modified silica tubes: preparation and cryogenic properties. *Chem Mater* 19:1939. <https://doi.org/10.1021/cm062540m>
- [9] Liu L, Lv F, Li P et al (2016) Preparation of ultra-low dielectric constant silica/polyimide nanofiber membranes by electrospinning. *Compos A Appl Sci Manuf* 84:292. <https://doi.org/10.1016/j.compositesa.2016.02.002>
- [10] Lv P, Dong Z, Dai X, Qiu X (2019) Flexible polydimethylsiloxane-based porous polyimide films with an ultralow dielectric constant and remarkable water resistance. *ACS Appl Polym Mater* 1:2597. <https://doi.org/10.1021/acsa.19b00484>
- [11] Bommer JC, Spikes JD (1991) Phthalocyanines: properties and applications. *Photochem Photobiol* 53:419. <https://doi.org/10.1111/j.1751-1097.1991.tb03651.x>
- [12] Martinez-Diaz MV, de la Torre G, Torres T (2010) Lighting porphyrins and phthalocyanines for molecular photovoltaics. *Chem Commun* 46:7090. <https://doi.org/10.1039/c0cc02213f>
- [13] Melville OA, Lessard BH, Bender TP (2015) Phthalocyanine-based organic thin-film transistors: a review of recent advances. *ACS Appl Mater Inter* 7:13105. <https://doi.org/10.1021/acsaami.5b01718>
- [14] Öztürk ZZ, Kılınç N, Atilla D, Gürek AG, Ahsen V (2009) Recent studies chemical sensors based on phthalocyanines. *J Porphyr Phthalocyanines* 13:1179. <https://doi.org/10.1142/S1088424609001522>
- [15] Panwar V, Kumar P, Ray SS, Jain SL (2015) Organic inorganic hybrid cobalt phthalocyanine/polyaniline as efficient catalyst for aerobic oxidation of alcohols in liquid phase. *Tetrahedron Lett* 56:3948. <https://doi.org/10.1016/j.tetlet.2015.05.003>
- [16] Higashino T, Imahori H (2015) Porphyrins as excellent dyes for dye-sensitized solar cells: recent developments and insights. *Dalton Trans* 44:448. <https://doi.org/10.1039/c4dt02756f>
- [17] Yang S, Yu Y, Gao X, Zhang Z, Wang F (2021) Recent advances in electrocatalysis with phthalocyanines. *Chem Soc Rev*. <https://doi.org/10.1039/D0CS01605E>
- [18] Wang Z, Gai S, Wang C et al (2019) Self-assembled zinc phthalocyanine nanoparticles as excellent photothermal/photodynamic synergistic agent for antitumor treatment. *Chem Eng J* 361:117. <https://doi.org/10.1016/j.cej.2018.12.007>
- [19] Achar BN, Fohlen GM, Parker JA (1982) Phthalocyanine polymers. IV. Novel type of thermally stable polyimides derived from metal phthalocyanine tetramines and benzophenone tetracarboxylic dianhydride. *J Polym Sci A Polym Chem* 20:2773. <https://doi.org/10.1002/pol.1982.170201004>
- [20] Shirai H, Kobayashi K, Takemae Y, Suzuki A, Hirabaru O, Hojo N (1979) Functional metal-porphyrzine derivatives and their polymers, 2. Synthesis and properties of polyimides containing metal-phthalocyanines. *Die Makromol Chem* 180:2073. <https://doi.org/10.1002/macp.1979.021800902>
- [21] Chen L, Ding Y, Yang T, Wan C, Hou H (2017) Synthesis and properties of a high dielectric constant copolymer of a copper phthalocyanine oligomer grafted to amino-capped polyimide. *J Mater Chem C* 5:8371. <https://doi.org/10.1039/C7TC03169F>
- [22] Georgiev A, Yordanov D, Dimov D, Assa J, Spassova E, Danev G (2015) Spectroscopic investigation of different concentrations of the vapour deposited copper phthalocyanine as a “guest” in polyimide matrix. *Spectrochim Acta A Mol Biomol Spectrosc* 140:444. <https://doi.org/10.1016/j.saa.2015.01.010>
- [23] Karaca H, Delibaş NÇ, Sağlam S et al (2021) Metallophthalocyanines derived with phenyl sulfide by bridging triazole using click chemistry: synthesis, computational study, redox chemistry and catalytic activity. *J Mol Struct* 1236:130225. <https://doi.org/10.1016/j.molstruc.2021.130225>
- [24] Augustine D, Vijayalakshmi KP, Sadhana R, Mathew D, Reghunadhan Nair CP (2014) Hydroxyl terminated PEEK-toughened epoxy–amino novolac phthalonitrile blends: synthesis, cure studies and adhesive properties. *Polymer* 55:6006. <https://doi.org/10.1016/j.polymer.2014.09.042>
- [25] Achar BN, Fohlen GM, Parker JA (1984) Studies on heat-resistant poly(metal phthalocyanine)-imide copolymers. *J Polym Sci A Polym Chem* 22:319. <https://doi.org/10.1002/pol.1984.170220204>
- [26] Achar BN, Fohlen GM, Lokesh KS (2003) Degradation study on the thermally stable nickel phthalocyanine sheet polymer. *Polym Degrad Stab* 80:427. [https://doi.org/10.1016/s0141-3910\(03\)00024-7](https://doi.org/10.1016/s0141-3910(03)00024-7)
- [27] Jung SH, Ha C-S (2006) Syntheses and characterization of polyimide containing metal phthalocyanine for organic electroluminescent devices. *High Perform Polym* 18:679. <https://doi.org/10.1177/0954008306068230>
- [28] Maya EM, de la Torre G, Lozano AE, Torres T, de la Campa JG, de Abajo J (2006) Novel cobalt(II) phthalocyanine-containing polyimides: synthesis, characterization, thermal and optical properties. *Macromol Rapid Commun* 27:1852. <https://doi.org/10.1002/marc.200600483>
- [29] Gu H, Gao C, Du A et al (2022) An overview of high-performance phthalonitrile resins: fabrication and electronic

- applications. *J Mater Chem C* 10:2925. <https://doi.org/10.1039/d1tc05715d>
- [30] Li K, Zheng P, Tong L et al (2019) Design and properties of poly(arylene ether nitriles) composites via incorporation of poly(arylene ether nitriles) grafted Fe₃O₄/Fe-phthalocyanine hybrid submicron-spheres. *Compos B Eng* 176:107202. <https://doi.org/10.1016/j.compositesb.2019.107202>
- [31] Yahya M, Nural Y, Seferoğlu Z (2022) Recent advances in the nonlinear optical (NLO) properties of phthalocyanines: a review. *Dyes Pigm* 198:109960. <https://doi.org/10.1016/j.dyepig.2021.109960>
- [32] Shen X, Lu W, Feng G, Yao Y, Chen W (2009) Preparation and photoactivity of a novel water-soluble, polymerizable zinc phthalocyanine. *J Mol Catal* 298:17. <https://doi.org/10.1016/j.molcata.2008.09.023>
- [33] Darwish WM, Darwish AM, Al-Ashkar EA (2015) Synthesis and nonlinear optical properties of a novel indium phthalocyanine highly branched polymer. *Polym Adv Technol* 26:1014. <https://doi.org/10.1002/pat.3520>
- [34] Yang S, Yu Y, Gao X, Zhang Z, Wang F (2021) Recent advances in electrocatalysis with phthalocyanines. *Chem Soc Rev* 50:12985. <https://doi.org/10.1039/D0CS01605E>
- [35] Furuyama T, Satoh K, Kushiya T, Kobayashi N (2014) Design, synthesis, and properties of phthalocyanine complexes with main-group elements showing main absorption and fluorescence beyond 1000 nm. *J Am Chem Soc* 136:765. <https://doi.org/10.1021/ja411016f>
- [36] Chen Y, Hanack M, Blau WJ et al (2006) Soluble axially substituted phthalocyanines: synthesis and nonlinear optical response. *J Mater Sci* 41:2169. <https://doi.org/10.1007/s10853-006-5552-9>
- [37] Suchan A, Nackiewicz J, Hnatejko Z, Waclawek W, Lis S (2009) Spectral studies of zinc octacarboxyphthalocyanine aggregation. *Dyes Pigm* 80:239. <https://doi.org/10.1016/j.dyepig.2008.06.009>
- [38] Zhang K, Yu Q, Zhu L et al (2017) The Preparations and water vapor barrier properties of polyimide films containing amide moieties. *Polymers* 9:677. <https://doi.org/10.3390/polym9120677>
- [39] Fu T, Guo M, Wang XL, Wang YZ (2020) In situ phthalocyanine synthesis chemistry in flames towards molecular fireproof engineering. *Chem Commun* 56:9525. <https://doi.org/10.1039/d0cc03899g>
- [40] Zhou H, Lei H, Wang J, Qi S, Tian G, Wu D (2019) Breaking the mutual restraint between low permittivity and low thermal expansion in polyimide films via a branched crosslink structure. *Polymer* 162:116. <https://doi.org/10.1016/j.polymer.2018.12.033>
- [41] Wang L, Yang J, Cheng W, Zou J, Zhao D (2021) Progress on polymer composites with low dielectric constant and low dielectric loss for high-frequency signal transmission. *Front Mater* 8:774843. <https://doi.org/10.3389/fmats.2021.774843>
- [42] Han S, Li Y, Hao F et al (2021) Ultra-low dielectric constant polyimides: combined efforts of fluorination and micro-branched crosslink structure. *Eur Polymer J*. <https://doi.org/10.1016/j.eurpolymj.2020.110206>
- [43] Cole KS, Cole RH (1941) Dispersion and absorption in dielectrics I Alternating current characteristics. *J Chem Phys* 9:341. <https://doi.org/10.1063/1.1750906>
- [44] Li X, Liu T, Jiao Y et al (2019) Novel high-performance poly(benzoxazole-co-imide) resins with low dielectric constants and superior thermal stabilities derived from thermal rearrangement of ortho-hydroxy polyimide oligomers. *Chem Eng J* 359:641. <https://doi.org/10.1016/j.cej.2018.11.175>
- [45] Zhang P, Zhang K, Chen X, Dou S, Zhao J, Li Y (2021) Mechanical, dielectric and thermal properties of polyimide films with sandwich structure. *Compos Struct* 261:1. <https://doi.org/10.1016/j.compstruct.2020.113305>
- [46] Çakmakçı E, Güngör A (2013) Preparation and characterization of flame retardant and proton conducting boron phosphate/polyimide composites. *Polym Degrad Stab* 98:927. <https://doi.org/10.1016/j.polymdegradstab.2013.03.003>
- [47] Zhang W, Li X, Guo X, Yang R (2010) Mechanical and thermal properties and flame retardancy of phosphorus-containing polyhedral oligomeric silsesquioxane (DOPO-POSS)/polycarbonate composites. *Polym Degrad Stab* 95:2541. <https://doi.org/10.1016/j.polymdegradstab.2010.07.036>

Publisher's Note Springer Nature remains neutral with regard to jurisdictional claims in published maps and institutional affiliations.

Springer Nature or its licensor holds exclusive rights to this article under a publishing agreement with the author(s) or other rightsholder(s); author self-archiving of the accepted manuscript version of this article is solely governed by the terms of such publishing agreement and applicable law.